Pressure-induced bond buckling in $YBa_2Cu_3O_{7-\delta}$

A. Sahiner, E. D. Crozier, and D. T. Jiang
Department of Physics, Simon Fraser University, Burnaby, British Columbia, Canada V5A 1S6

R. Ingalls
Department of Physics, Box 351560, University of Washington, Seattle, Washington 98195

(Received 17 July 1998)

Cu *K*-edge extended x-ray-absorption fine-structure (EXAFS) measurements of $YBa_2Cu_3O_{7-\delta}$ ($\delta=0.05$) at atmospheric pressure and at 3.4, 11.4, 31.8, and 65 kbar are presented. The experiments were performed isothermally at 80 K. In the EXAFS region, the Cu(1)-O(4)-Cu(2) path is enhanced by focused multiple scattering. Analysis indicates a buckling of this path due to out-of-line movement of the O(4) atom. The forward scattering angle β shows a rapid increase at low pressures and then saturates at 65 kbar to an angle (as large as) 12° depending upon the buckling model used in the EXAFS analysis. Analysis of x-ray-absorption near-edge structure data taken for the $\delta=0.9$ and $\delta=0.05$ compounds shows a decrease in the amplitude of the spectral feature associated with the Cu(1) atom in the $\delta=0.9$ compound indicating that the amount of pressure-induced charge transfer from Cu(1) to Cu(2) is of the order of 0.0007 holes/kbar [S0163-1829(99)03702-9]

I. INTRODUCTION

Pressure-related structural changes in $YBa_2Cu_3O_{7-\delta}$ have been previously investigated by x-ray diffraction,[1–4] neutron diffraction,[5] and x-ray-absorption fine structure (XAFS) (Ref. 6) at room temperature. The main interests were on the changes in the interatomic distances between copper and oxygen atoms in the CuO_2 planes and in the CuO chains and the compressibility anisotropies in the unit cell along its crystallographic axes. Fietz, Dietrich, and Ecke,[1] applying pressure up to 120 kbar to $YBa_2Cu_3O_{7-\delta}$ used x-ray diffraction (XRD) to investigate the response of the crystal along its axes, and suggested two different models in interpreting their data. One model assumed a strong compression along the *c* axis, whereas the other assumed a strong decrease in length of the *b* axis. Jorgensen *et al.*[5] applying hydrostatic pressure up to 5.78 kbar used neutron diffraction to investigate the correlation between the bond lengths and the amount of the charge transfer from the CuO chains to the CuO_2 planes. The slope of the *c* axis vs pressure curve from Jorgensen's data is twice that obtained by Fietz leading to a larger compressibility for $YBa_2Cu_3O_{7-\delta}$. However usually the low pressure compressibility measurements tend to give a higher compressibility due to the decrease of the compressibility with increasing pressure.[5]

In two independent high-pressure XRD experiments on $YBa_2Cu_3O_{7-\delta}$ a structural phase transition (orthorhombic → tetragonal) was reported above 70 kbar.[4,7] The compression along the *b* axis relative to the *a* axis is different for these two separate measurements, and while the data of Jaya, Natarajan, and Rao[4] (obtained by angle dispersive XRD) show a sudden jump in the *b*-axis parameter just above 65 kbar, the data of Akhtar, Akhtar, and Catlow[7] (obtained by energy dispersive XRD) indicate a smooth transition from orthorhombic to tetragonal symmetry. Both of these data suffer from the low-angle–energy resolution. It was noted that a number of reflections that are actually nondegenerate in the tetragonal symmetry have merged in the high pressure data due to the low resolution of the energy-dispersive spectrum[4] making the claim of a phase transition questionable.

Almost all the previous high-pressure structural characterizations on $YBa_2Cu_3O_{7-\delta}$ assume a uniform compression along the *c* axis with pressure. However the chain copper-apical oxygen [Cu(1)-O(4)] and the planar copper-apical oxygen [Cu(2)-O(4)] bonds respond differently to the applied pressure.[5] It was proposed that due to the relative stiffness of Cu(1)-O(4) bonds with respect to the Cu(2)-O(4) bonds, only the latter compress with pressure along with the *c*-axis compression.[5] It was also assumed that O(4) remains along the *c*-axis although no thermal ellipsoids were reported to support this.

A number of studies reported conflicting results in the anomalies of the apical oxygen position. A temperature-dependent anomaly, namely, a small discontinuity (~0.02 Å) in the Cu(1)-O(4) bond length near T_c was reported by Shafer *et al.*,[8] but not observed by others.[9,10] Mustre de Leon and co-workers,[11,12] using extended x-ray-absorption fine structure (EXAFS), observed a split O(4) position ($\delta R = 0.13$Å) distribution along the *c* axis and indicated that the split position appeared to decrease around T_c. According to subsequent temperature-dependent EXAFS measurements on oriented powders,[13] and single crystals and oriented thin films[14] of $YBa_2Cu_3O_{7-\delta}$, the split O(4) position is sample dependent. Later, Schweiss *et al.*,[15] applying neutron diffraction on single crystals of $YBa_2Cu_3O_{7-\delta}$ investigated the mean square displacements of the individual atoms in $RBa_2Cu_3O_{7-\delta}$ (R=Y, Ho) and reported no evidence of the anomalous vertical displacement of the O(4) atom around T_c. However, they found static contributions to the displacements within a plane containing the apical O(4) atoms. This plane is parallel to the *ab* plane. Inelastic neutron scattering measurements[16] indicated a shift of the apical O(4) atoms along the ⟨110⟩ direction from the original position around T_c, causing a local distortion associated with the buckling structure similar to the one observed in the orthorhombic phase of $La_{2-x}Sr_xCuO_4$ (Ref. 17) and $La_{2-x}Ba_xCuO_4$.[18]

Pressure has been reported to cause buckling in some perovskite related compounds. For example, in the high pressure EXAFS study of $La_{2-x}Sr_xCuO_4$ (Ref. 6) buckling of the Cu-O-Cu bonds with increasing pressure was observed. Similar displacements of the bridging oxygen atoms in the ReO_3 system have been reported by neutron diffraction[19] and EXAFS (Refs. 20 and 21) experiments. ReO_3 goes through a second order phase transition around 5 kbar, in which the ReO_6 octahedra rotate about the [111] axes.[22,23] This transformation results in the buckling of the Re-O-Re bond around the oxygen atom. The forward scattering amplitude $f(\beta,k)$ of the ''focused'' Re-O-Re multiple scattering (MS) path is very sensitive to the scattering through the angle β, measured from the oxygen atom and decreases sharply with increasing values of it. Its effect on the Fourier transformed EXAFS data is the reduction of the amplitude of the Re-O-Re MS peak (at $R\sim 3.6$Å). Houser *et al.*,[21] using the reduction in the amplitude of the MS peak calculated the bridging angle across the oxygen atom. In their fits to the data at $P=1$ bar, they used the fact that the XAFS signal from a dynamical situation in which the center atom in a linear link vibrates with a certain mean-square displacement from the line is equivalent to the center atom being statically displaced by the rms value, provided the dynamic variation is symmetric about the line, and find the bridging angle to be 172°. At 17 ± 3kbar they found the bridging angle to become $164\pm 2°$ taking the starting point of their fits for the bridging angle as 172° at a pressure of 1 bar.

In this study, our focus is on the pressure-induced displacements of the O(4) atoms in the Cu(1)-O(4)-Cu(2) unit. In order to obtain reliable structural information about the O(4) sites using EXAFS data, one has to identify the experimental peaks associated with the scattering paths involving O(4) atoms in the Fourier transformed data. Previously, Di Cicco and Berrettoni[24] applied multiple scattering analysis to study the angle distribution of the Cu-O-Cu bonds in $YBa_2Cu_3O_{7-\delta}$, and $Bi_2Sr_2CaCu_2O_8$ high-T_c compounds. The focus of their analysis was on the Cu-O-Cu paths (parallel to the *ab*-plane), and the contribution of the apical Cu-O-Cu (parallel to the *c* axis) was ignored. Using the FEFF6.10 (Refs. 25 and 26) multiple scattering analysis code we have identified the peak at 3.90 Å in the Fourier transform to be associated with the Cu(1)-O(4)-Cu(2) MS peak. Due to the EXAFS phase shift this is shorter than the actual spatial separation 4.12 Å of the Cu(1) and Cu(2) atoms. The experimental data show a decrease in the intensity of this peak with increasing pressure. We attribute this reduction to the decrease in the amplitude of the forward scattering at the oxygen atom site resulting from the relative displacement of these bridging oxygen perpendicular to the *c* axis. Using the scattering amplitude and phases calculated by FEFF at various buckling angles as the standards we apply nonlinear least squares fits to the Cu(1)-O(4)-Cu(2) MS peak and analyze the evolution of the bond angle with pressure.

The Cu *K*-edge x-ray-absorption near-edge structure (XANES) of $YBa_2Cu_3O_{6.10}$ and $YBa_2Cu_3O_{6.95}$ are also presented. The spectral feature about 1 eV above the edge corresponds to the monovalent Cu(1) atoms[27–30] and its intensity variation can be used as a probe to the charge transfer from the CuO chains to the CuO_2 planes. Comparing the XANES of $YBa_2Cu_3O_{6.10}$ and $YBa_2Cu_3O_{6.95}$, we obtain a relation between the number of holes transferred to the planes and the area of this feature to estimate the change in the number of the holes per CuO_2 plane by pressure. Our results suggest an increase in the amount of 0.0007 ± 0.0002 holes/kbar which, within experimental error, is in agreement with the reported neutron diffraction results[5] using the bond valence sum technique.

We begin with the description of the experiment in Sec. II. The data analysis methods are described in Sec. III. The EXAFS and XANES results are discussed in Sec. IV and the conclusions are summarized in Sec. V.

II. EXPERIMENT

The $YBa_2Cu_3O_{7-\delta}$ samples were prepared using starting materials of $BaCO_3$, Y_2O_3, and CuO. The powders were repeatedly ground in an automatic grinder, sifted through a 75 μm sieve, packed into high purity MgO crucibles and calcined in air for 18 h. This process was repeated 10 times. Each time, the temperature was increased by 10 °C. A final calcining was done in very pure oxygen at 925 °C. Then the powder was pressed into 3/4 in. diameter, 3 g pellets and sintered in very pure oxygen. The tube was slowly cooled over a period of two days to fully oxygenate the pellets.[31] The midpoint of the superconducting transition for the sample was 93.4 K.[31] The oxygen content was determined by examining the room temperature electrical conductivity of a series of deoxygenated pellets which were prepared to have an oxygen content about $\delta=1.0$. By plotting the room temperature conductivity versus δ for a series of samples and by assuming that at $\delta=1.0$, $YBa_2Cu_3O_{7-\delta}$ is an insulator a δ value for the fully oxygenated pellets was obtained.[31] The $\delta=0.9$ samples were prepared deoxygenating the fully oxygenated samples via a cryogenically assisted volumetric titration apparatus (gas handling system) presented in Ref. 31.

The high-pressure x-ray-absorption data were collected on beamline IV-I at the Stanford Synchrotron Radiation Laboratory. A Si(111) double crystal monochromator was used and detuned to 50% of the maximum intensity to reduce the harmonic content of the beam. The pressure to the samples was applied through mechanically driven polycrystalline B_4C anvils in a pressure cell designed for the low-temperature measurements.[32,33] The samples were first cooled to liquid-nitrogen temperatures and then the pressure was applied to maintain an isothermal compression.

III. DATA ANALYSIS

The data reduction steps in the analysis of the EXAFS signal data were performed in the conventional way and order:[34,35] background subtraction, *k*-space conversion, Fourier transformation, and nonlinear least squares fit to the data to extract the structural parameters. The background signal was subtracted from the data using the program AUTOBK (Ref. 36) which subtracts a linear background from a pre-edge fit, normalizes the data to the absorption edge jump, and then uses fourth-order polynomial splines connected at equally spaced knots in *k* space for the post-edge background. It minimizes the difference between the experimental data and a theoretical standard over the low-*R* region, thereby reducing the leakage from the first shell to this re-

TABLE I. Pressure calibration from Ge bond compression. ΔR and V/V_0 were obtained from (a) the phase difference method applied to the nearest-neighbor distance R_1 and (b) a five shell nonlinear least squares fit to the Fourier transform of $k\chi(k)$ using FEFF calculated standards including multiple scattering paths. From the multishell fits $R_1=2.447$ Å at 1 bar, $E_0=1.4$ eV and $\sigma_I^2=0.0028$ Å^2 were obtained as described in the text.

	Phase difference method			Multishell fit		
Exp. no.	ΔR_1(Å)	V/V_0	P(kbar)	ΔR_1(Å)	V/V_0	P(kbar)
1	0.006	0.992	3.40	0.006	0.992	3.40
2	0.012	0.985	11.4	0.012	0.985	11.4
3	0.030	0.964	29.6	0.032	0.960	31.8
4	0.045	0.945	62.5	0.049	0.940	65.0
Error	±0.01		±5.0	±0.01		±5.0

gion. The standards used in the background subtraction routine were calculated by FEFF6.10. After the background subtraction the EXAFS interference function $[\chi(k)]$ was obtained by converting from the x-ray energy (E) to the photoelectron wave vector (k) by $k=2\pi/h\ [2m(E\text{-}E_0)]^{1/2}$ while setting the threshold energy E_0, at the first inflection point (first maximum in the first derivative spectra). All the Fourier transformations of the $\chi(k)$'s were performed using a 10% Gaussian window and applying a k weighting.

Ge K-edge EXAFS was used as the calibrant to calculate the pressures applied to the $YBa_2Cu_3O_{7-\delta}$ sample. The large separation between the first neighbor $R_1=2.447$ Å, and the second nearest neighbor $R_2=3.996$ Å, permits a simple and accurate determination of the compression of R_1 using the phase difference method[34,35] and has no complications due to MS. The first shell of Ge in the $k\chi(k)$ transform (1.75–14.40 Å^{-1}) was selected (1.50–2.88 Å) and the total phase $\Phi=2kR_1+\delta(k,R_1)$ obtained by taking the inverse transform. For the low pressures involved the EXAFS phase shift $\delta(k,R_1)$ is independent of pressure. The difference between $\Phi(R_1,P)$ at pressure P and at 1 bar was fitted to a straight line over the range 4.4–9.6 Å^{-1}. The slope of $\Delta R(P)=R_1(P)-R_1$ (1 bar) is listed in Table I.

In this paper our emphasis is on the higher shells of $YBa_2Cu_3O_{7-\delta}$ where MS must be included. To provide an indication of accuracy with which this can be done with the FEFF6.10 MS code, $\Delta R(P)$ of Ge was also determined by a multishell fit for $R\leqslant 4.80$ Å. A theoretical model including the multiple scattering paths was calculated for the Ge K-edge data by FEFF. The sum of the individual contributions of the different scattering paths is expressed in a form, analogous to the EXAFS equation, as

$$\chi(k)=\sum_{\Gamma}\frac{N_\Gamma S_0^2}{kR_\Gamma^2}\,|f_{\rm eff}^{\Gamma}(k)|e^{-2k^2\sigma_\Gamma^2}e^{-2R_\Gamma/\lambda(k)}\times\sin[2kR_\Gamma+\phi_\gamma(k)+2\delta_c(k)],\qquad(1)$$

where Γ is the path label, N is the degeneracy of the path Γ, k is the wave vector, R_Γ is the effective path length ($R=r_{\rm tot}/2$), $f_{\rm eff}^{\Gamma}$ is the effective scattering amplitude, S_0^2 is a many body correction factor, $\phi_\Gamma(k)$ is the net scattering phase shift, $\delta_c(k)$ is the central atom phase shift, σ_Γ^2 is the mean square variation in R for path Γ, and λ is the mean free path term. Here the summation was restricted to those with curved wave amplitude >4% of the amplitude of the largest and with effective path length $R\leqslant 4.69$ Å. There are five paths; three single scattering involving the first, second and the third nearest neighbor and two MS. The MS paths are the triangular paths corresponding to

$$(000)\left(\frac{-a\sqrt{3}}{4}\,\frac{a\sqrt{3}}{4}\,\frac{a\sqrt{3}}{4}\right),$$

$$\left(\frac{-a\sqrt{3}}{4}\,\frac{-a\sqrt{3}}{4}\,\frac{-a\sqrt{3}}{4}\right),$$

and

$$(000)\left(\frac{a\sqrt{3}}{4}\,\frac{a\sqrt{3}}{4}\,\frac{-a\sqrt{3}}{4}\right)\left(\frac{a}{2}\,\frac{a}{2}\,0\right)$$

atoms, where a is the lattice parameter for the diamond structure.

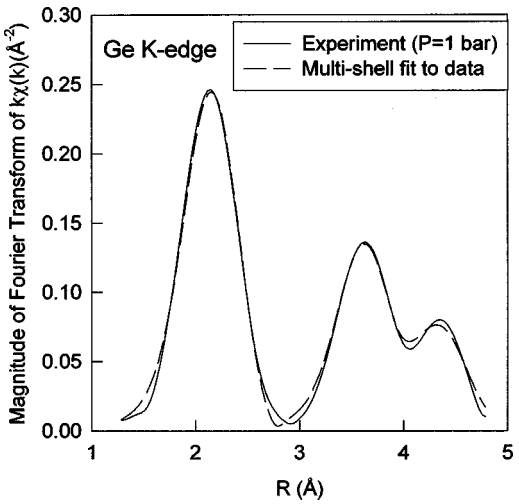

FIG. 1. Magnitude of the Fourier transform of $k\chi(k)$ for the Ge K edge at 80 K at atmospheric pressure and fit to the data. The data were transformed over the range 1.75–14.40 Å^{-1} using a 10% Gaussian window.

The model calculated by FEFF was used as the standard in a first five shell nonlinear least squares fit to the imaginary part and the magnitude of the complex Fourier transform (FT) of the $k\chi(k)$ by the program EXAFIT based on the Levenberg-Marquardt algorithms.[32,37] In Fig. 1, the FT of the Ge EXAFS and fit to the data are shown. During the fit procedure first N_1 is fixed at 4.0 (with S_0^2 set at 0.8), N_n/N_1 and R_n-R_1 were constrained to their crystallographic value in the shells. E_0, the Debye-Waller factors (σ_n^2) for all the shells and R_1 were varied. In this way the E_0 and σ_1^2 are obtained. Then fixing E_0 and σ_1^2 and keeping the ratios of the coordination numbers and the differences in the near-neighbor distances constant, but varying R_1 and N_1 the Ge-Ge nearest-neighbor distances (R_1) were obtained. The lattice parameters were determined from R_1 and the corresponding changes in the volume V with respect to the atmospheric pressure V_0 were calculated. Using the equation of state curves,[38] the pressure values corresponding to these

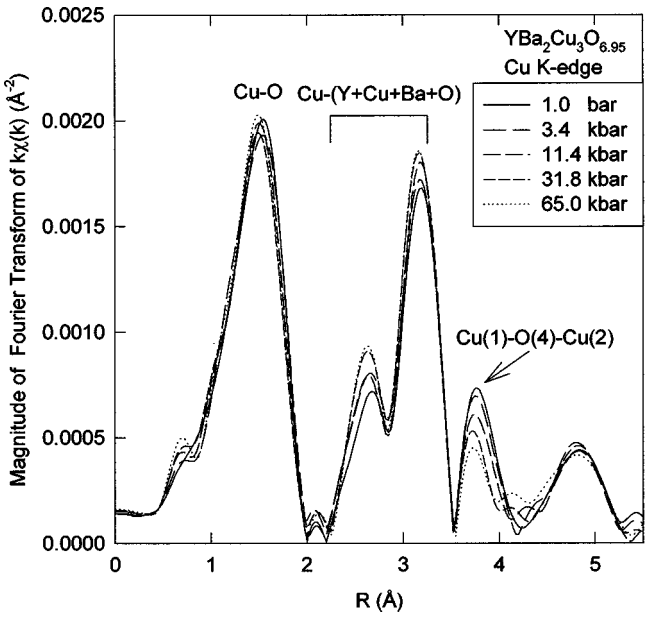

FIG. 2. Magnitude of the Fourier transform of $k\chi(k)$ for the Cu K edge in $YBa_2Cu_3O_{6.95}$ at 80 K under different pressures. The data were transformed over the range 2.65–14.55 $Å^{-1}$ using a 10% Gaussian window.

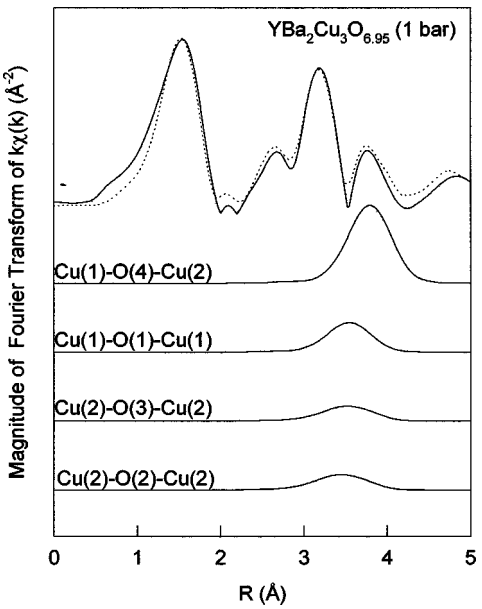

FIG. 3. Magnitude of the Fourier transform of $k\chi(k)$ for the Cu K edge in $YBa_2Cu_3O_{6.95}$ at 80 K at 1 bar (solid line), theoretical model calculated by FEFF6.10 (dotted line) and the magnitude of the Fourier transform of $k\chi(k)$ due to Cu-O-Cu scattering paths. The data and model were both transformed over the range 2.65–14.55 $Å^{-1}$ using a 10% Gaussian window.

volume changes were determined. As shown in Table I, the ΔR from the phase difference method and multishell fitting are in good agreement.

IV. RESULTS AND DISCUSSION

A. EXAFS

The FT data for the $YBa_2Cu_3O_{7-\delta}$ under different pressures are shown in Fig. 2. The maximum pressure used in the experiment was 65 kbar. The experimental peaks are labeled according to their scattering atoms. This labeling was done according to the MS modeling results from FEFF. It is normally expected that the pressure will increase the magnitude of the peaks in the FT data. This is due to the decrease of the compressibility and consequently the increase in magnitude of the Debye-Waller factor $\exp(-2k^2\sigma^2)$. It is expected to have a larger effect for the peaks corresponding to more distant neighbors. In Fig. 2 small changes in Cu-O peaks but large and consistent intensity increase in Cu-(Y+Cu+Ba+O) peaks are evident. However, the significant decrease in the amplitude of the Cu(1)-O(4)-Cu(2) peak with pressure can be explained by the multiple scattering effects. In Fig. 3, the FT data for the $YBa_2Cu_3O_{6.95}$ at 1 bar, the FEFF model, and the individual Cu-O-Cu multiple scattering contributions are shown. The amplitude of the Cu(1)-O(4)-Cu(2) contribution is larger than for the other Cu-O-Cu paths. In the former the forward scattering is enhanced by the linear path whereas the latter are already reduced at 1 bar having a $\beta \cong 15°$ and the $f(\beta,k)$ is reduced. Lattice parameters for the crystal structure were obtained from the neutron diffraction results at 80 K.[10] The lattice parameters for the higher pressures were calculated using the XRD results.[1]

For the $YBa_2Cu_3O_{7-\delta}$, the FEFF calculations were performed by taking Cu(1) and Cu(2) atoms as the central absorbing atom, respectively. The $\chi(k)$'s resulting from these separate calculations were combined with a weight ratio of 1:2 for $[\chi(k)]_{Cu(1)}$: $[\chi(k)]_{Cu(2)}$. The direct output from FEFF6.10 using these parameters leads to significant deviations from the intensities of the peaks of the experimental FT data. These discrepancies are mainly caused by the uncertainties in the Debye-Waller factor and the amplitude reduction factor S_0^2. The correlated Debye Model used in FEFF works well for the linear paths in metals[26] but is not a good approximation for linear paths in perovskites. In the treatment of the dynamical motion of a MS path, FEFF introduces a phenomenological Debye-Waller factor for the average MS path with the atoms in fixed positions. The neglect of angular correlations, particularly for triangular paths[39–41] can introduce errors.[26] The uncertainty in S_0^2 is ~20% in Ref. 26. Testing FEFF results for a number of standards, Li *et al.*,[42] noted that $S_{0\,\mathrm{eff}}^2$ (which also includes the ''mean-free path'' term, $\exp[-2R/\lambda(k)]$) can vary by 10–15% depending on the local chemical environment of the absorbing atom. Therefore in creating the theoretical model for the experimental data, S_0^2 and the σ^2 are adjusted by using a nonlinear least squares fitting routine WINXAS.[43]

Knowing the amplitudes and the phase shifts from all of the significant scattering paths provides an important advantage in the correct labeling of the experimental peaks in FT data. The closeness of the several scattering paths in length makes it difficult to identify the peaks, and for the multiple scattering paths, the large phase shifts might bring additional uncertainty in labeling. In Fig. 2, the data has been divided into three regions and the peaks were labeled with guidance from the FEFF model. There are five different Cu-O bonds in the crystal structure contributing to the first region. These are Cu(1)-O(4), Cu(1)-O(1), Cu(2)-O(2), Cu(2)-O(3), and Cu(2)-O(4) in the order of their bond length. Previous EXAFS stud-

ies in this region reported a two-site location for the O(4) atom with the separation of 0.13 Å away from T_c.[11,12] It was reported[11] that this separation decreases by 0.02 Å around T_c according to the fits to Cu(1)-O(4) and Cu(2)-O(4) near-neighbor distances. Later Booth *et al.*[14] used polarization-dependent EXAFS measurements of a single crystal and an oriented thin film of $YBa_2Cu_3O_{7-\delta}$ to test the reported O(4) splitting. Though the single crystal data were best described by the split O(4) position, the thin film did not show any evidence of two-site axial oxygen. Our results did not show any consistent effects of pressure in the magnitude of these peaks and given that our sample was polycrystalline, the five different Cu-O distances in close proximity makes a quantitative analysis unreliable in this region. Another complicated region in the analysis of polycrystalline $YBa_2Cu_3O_{7-\delta}$ is between 2.3 and 3.6 Å; according to FEFF there are 19 important scattering paths contributing to this region. In the previous studies at atmospheric pressure, the data in this region was fit by combining several paths into one to reduce the number of paths and the free parameters.[44] As mentioned earlier, our results show an increase in the magnitude of the peaks of the FT data with an increase in the pressure.

Our concern is the region between 3.6–4.1 Å. According to the FEFF calculations there is a large contribution to this region from the Cu(1)-O(4)-Cu(2) multiple scattering path. Figure 4(a) shows an overlay of the $\chi(k)$ including all paths (with cw amplitude ratio $>4\%$ for $R \leqslant 5.8$ Å) and the $\chi(k)$ excluding the Cu(1)-O(4)-Cu(2) (apical) path. As shown in Fig. 4(a) the difference plot of the two $\chi(k)$ is significant. Excluding the MS path causes a large reduction in the magnitude of the peak in the FT around 3.9 Å as shown in Fig. 4(b). Accompanying this is a widening of the peak (located at 3.6 Å) due to a reduction of the interference between the in-plane [Cu(2)-O(2,3)-Cu(2) and Cu(1)-O(1)-Cu(1)] and the apical Cu-O-Cu paths. Previous EXAFS analysis of $YBa_2Cu_3O_{7-\delta}$ in this region[24,44] ignored the contribution of the Cu(1)-O(4)-Cu(2) path, and only the Cu(2)-Cu(2) and Cu(1)-Cu(1) pairs and the remaining Cu-O-Cu paths[24] were used in the fits to the data. Focused multiple scattering for the Cu(1)-O(4)-Cu(2) path was included in earlier work,[45] but was limited by using only a plane wave approximation for the forward scattering. The FEFF MS calculations, which use the curved wave approximation, indicate that the scattering amplitude due to Cu(1)-O(1)-Cu(1) and Cu(2)-O(2,3)-Cu(2) paths should peak around 3.6 Å, in the Fourier space as shown in Fig. 3. In the same figure the Cu(1)-O(4)-Cu(2) peak is shown to be around 3.9 Å, which matches the experimental peak position. Therefore we claim that the FT peak around 3.9 Å is primarily due to the apical Cu(1)-O(4)-Cu(2) scattering as also indicated in the single crystal and the thin film $YBa_2Cu_3O_{7-\delta}$ EXAFS studies of Booth *et al.*[14]

As opposed to the expected increase due to the pressure effect we observe a consistent decrease in the magnitude of the Cu(1)-O(4)-Cu(2) peak with pressure in the FT data. This decrease is significant (as shown in Fig. 2) and can be explained by the multiple scattering effects as in the EXAFS analysis of ReO_3 (Refs. 20 and 21) and $La_{2-x}Sr_xCuO_4$.[6] By analogy with these systems, the reduction in the magnitude of the FT peak corresponding to the Cu(1)-O(4)-Cu(2) path can be explained by the reduction in the scattering amplitude at the oxygen site due to the deviation of the bridging angle

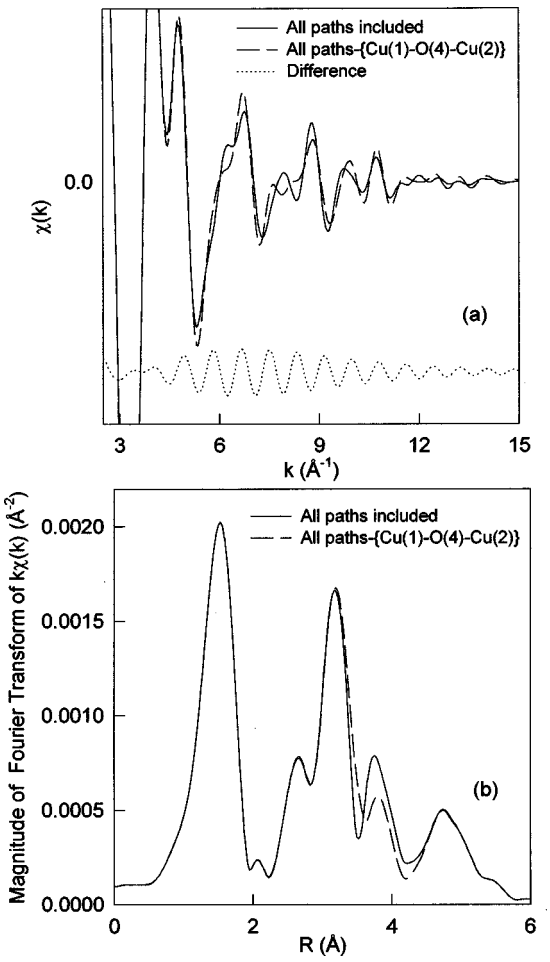

FIG. 4. (a) $\chi(k)$ of the FEFF model for $YBa_2Cu_3O_{6.95}$ including all the paths, all paths excluding the Cu(1)-O(4)-Cu(2) path and the difference of the two curves. (b) Magnitude of the Fourier transform of $k\chi(k)$ of the FEFF model for $YBa_2Cu_3O_{6.95}$ including all the paths and all paths excluding the Cu(1)-O(4)-Cu(2) path. The models were transformed over the range 2.65–14.55 $Å^{-1}$ using a 10% Gaussian window.

from 180°. The maximum scattering amplitude occurs for the ''focused'' path in which the Cu-O-Cu bonds are linear.

In order to examine the buckling in the apical Cu-O-Cu bonds we consider two models for the structural effect of increasing pressure. In model 1 we assumed that there was no buckling along the *c* axis, just compression. The compressions along the *a, b,* and *c* axes under pressure were calculated using previous XRD and neutron diffraction studies.[1,6] According to the neutron diffraction results, the main contraction for the apical Cu-O-Cu bond is in the softer Cu(2)-O(4) bond. The relatively stronger Cu(1)-O(4) bond does not show much change under pressure. This information was used in the calculations (i.e., $R_{\mathrm{Cu(1)\text{-}O(4)}}$ was kept constant at its ambient pressure value 1.856 Å and $R_{\mathrm{Cu(2)\text{-}O(4)}}$ was compressed along with the *c*-axis compression) and the models corresponding to pressures of 1 bar, 3.4, 11.4, 31.8, and 65 kbar were calculated. The results are shown in Fig. 5. In the second model, a buckling through the O(4) atom was assumed. Here again, the stiffness of the Cu(1)-O(4) bond with respect to Cu(2)-O(4) was taken into account and it was kept fixed while the Cu(2)-O(4) bond was allowed to compress. In order to produce the buckling, the O(4) atom was dis-

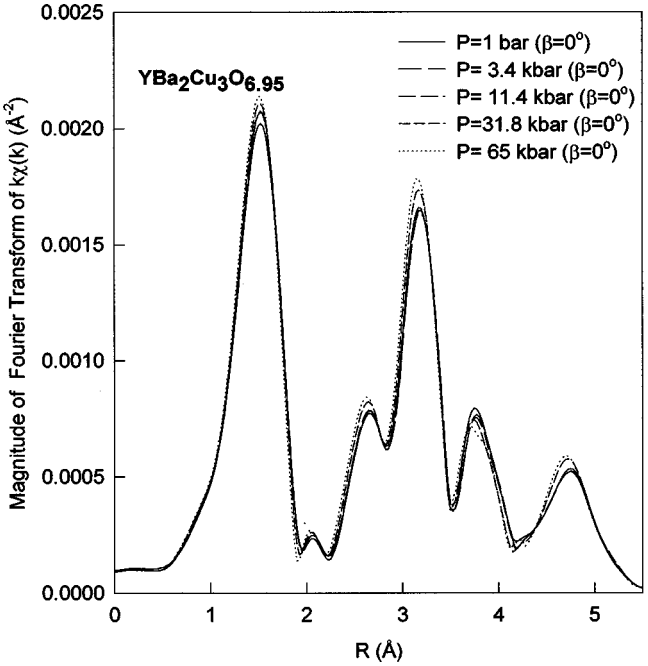

FIG. 5. Magnitudes of the Fourier transforms of $k\chi(k)$ of the FEFF models for $YBa_2Cu_3O_{6.95}$ at different pressures assuming a compression without buckling in the Cu(1)-O(4)-Cu(2) units. All the transforms were performed over the range 2.65–14.55 $Å^{-1}$ using a 10% Gaussian window.

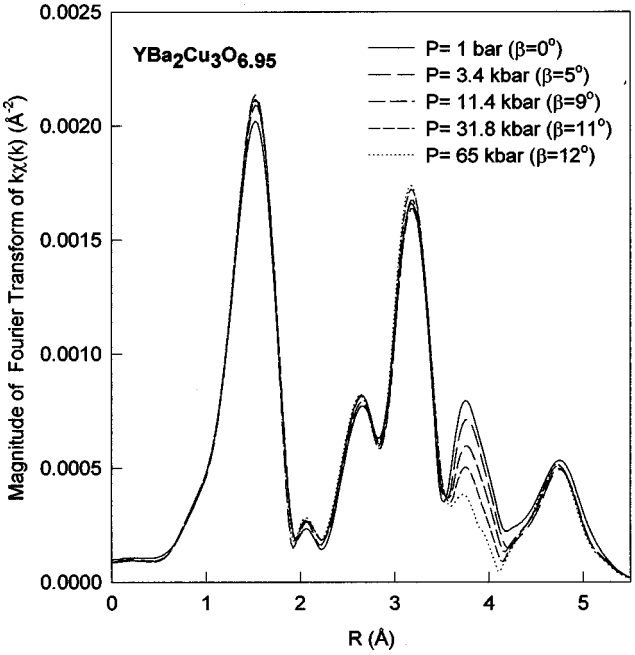

FIG. 6. Magnitudes of the Fourier transforms of $k\chi(k)$ of the FEFF models for $YBa_2Cu_3O_{6.95}$ at different pressures assuming a compression with buckling in the Cu(1)-O(4)-Cu(2) units. All the transforms were performed over the range 2.65–14.55 $Å^{-1}$ using a 10% Gaussian window.

placed along the *b* axis with increasing pressure. The *b* axis was selected because the compressibility of the *b* axis is known from the diffraction data to be greater than for the *a* axis. However the multiple scattering depends only on the polar angle the O(4) makes with the *c*-axis and from the EXAFS viewpoint it is not possible with polycrystalline samples to distinguish the direction in which the O(4) is displaced. The overall contraction of the Cu(1)-Cu(2) was restrained to be consistent with the XRD results. The results of these calculations are shown in Fig. 6.

To facilitate the simulations for Figs. 5 and 6, the FT data were divided into the three regions (0.0–2.3, 2.3–3.6, and 3.6–4.1 Å) as indicated earlier. The S_0^2 and individual σ^2's for the scattering paths for these simulations were obtained from the region-by-region fits to the data at atmospheric pressure. The σ^2's were then used to modify those calculated by FEFF. These modifications were transferred to the FEFF calculations at higher pressure. Since the total number of scattering paths is very large in the region-by-region fits, only the ten paths in each region having the largest contributions were used. For both the buckling and nonbuckling models, the expected pressure effects in the first two regions are noticed. The Cu-O peaks located at 1.5 Å, and the peaks in the 2.3–3.5 Å region show an increase in magnitude with pressure and a shift to the lower *R* values. But in the region (3.6–4.1 Å) the two models produce different results. In Fig. 5, the nonbuckling calculations indicate a shift towards the lower *R* values but do not reflect a large change in the magnitude of the FT peak. In Fig. 6, the model assuming a buckling in the apical Cu-O-Cu bonds indicates a strong pressure dependence of the Cu(1)-O(4)-Cu(2) peak. As in the case of the experimental data, the peak loses magnitude consistently with decreasing bridging angle (or increasing forward scattering angle β) and shifts towards lower *R*. We have used these buckling simulations in order to calculate the corresponding β values. The filled circles in Fig. 7 show a plot of β versus the pressure values used in the experiment. The β has a decreasing slope with increasing pressure saturating at 12° at 65 kbar. A quantitative calculation of β becomes less reliable at the higher angles because of the contributions from the other paths as indicated in Fig. 4.

In principle, the MS EXAFS fitting should be performed by calculating the MS paths over the distribution of positions of the Cu(1), O(4), and Cu(2) atoms.[39–41] But the fits are

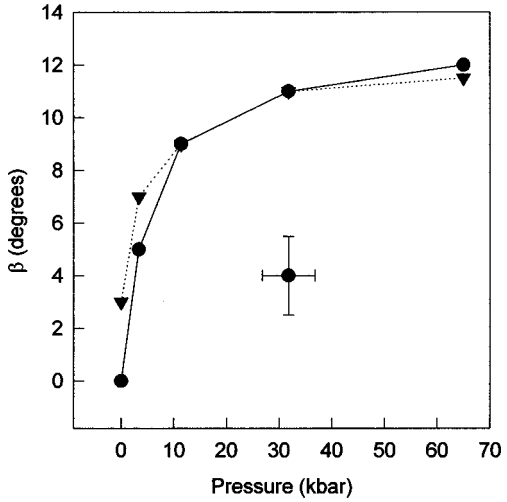

FIG. 7. The change in the forward scattering angle, β, versus pressure for $YBa_2Cu_3O_{6.95}$ determined with the buckling model for different starting values of β at 1 bar: $\beta=0°$ (filled circles), $\beta=3°$ (filled triangles).

sensitive to the correlated modes of motion of the atoms. We do not know the pressure dependence of the modes and different models for the distribution function will give different β. At pressures greater than 1 bar the β are overestimated due to neglect of the dynamical motion.[39,40] We can estimate the error using ion channeling and neutron diffraction results at atmospheric pressure. Neutron diffraction studies have measured the mean square displacement (MSD) of the O(4) atom at temperatures near 80 K (Refs. 9, 10, and 15) from which we estimate β to be $\sim 4°$. Schweiss *et al.*[15] separate the MSD into lattice dynamical and static displacements of the O(4) atom giving an equivalent static β of $\sim 2°$. Ion channeling studies[10,46] find the Cu and O atoms (along the *c* axis) have correlated displacements perpendicular to the *c* axis of ~ 0.04 Å (with a $\beta \sim 2°$) which would tend to decrease the XAFS-determined buckling angle. In order to take these effects into account we performed another set of calculations with the buckling model (model 2) starting with a 3° offset to β at 1 bar. In Fig. 7, the triangles correspond to the values of β obtained in this new model. The values obtained in the fitting at pressures greater than 1 bar depend upon the initial starting value of β at 1 bar. Since in our analysis method we can not distinguish between static and dynamic contributions to β at atmospheric pressure and since we do not know the pressure dependence of the distributions, the saturation value of β at 65 kbar may be overestimated by as much as 3°.

In summary, the effect of pressure is to induce a buckling of the Cu(1)-O(4)-Cu(2) chain of atoms by an out-of-line displacement of the O(4) atom. Within the accuracy of the present EXAFS analysis the buckling angle at the highest pressure measured is less than 12° and more than 8.5°.

B. XANES

Although the existence of the pressure-induced charge transfer from the CuO chains to CuO_2 planes has been generally accepted, there is no agreement on the amount of the holes that are transferred.[5,47–49] Jorgensen *et al.*, using bond-valence-sums in their neutron diffraction data of $YBa_2Cu_3O_{6.93}$ obtained a charge transfer of 0.00065 holes/kbar per CuO_2 plane.[5] Gupta and Gupta's electronic structure calculations using the tight binding recursion method[48] reported a transfer of 0.00035 holes/kbar per CuO_2 plane for fully oxygenated ($\delta = 0$) compound. Almasan *et al.*,[47] using a phenomenological model relating the T_c to the number of holes per CuO_2 plane, obtained a value of 0.0003 holes/kbar from the analysis of their data for the pressure dependence of T_c in $YBa_2Cu_3O_{\approx 7}$. Reyes *et al.*,[49] using a charge transfer model in interpreting the high pressure nuclear-quadrupole-resonance, reported a change of 0.0006 holes/kbar per CuO_2 plane.

In Fig. 8 Cu *K*-edge XANES of $YBa_2Cu_3O_{7-\delta}$ ($\delta = 0.9$ and 0.05) at 1 bar and 65 kbar are shown. A linear background from the pre-edge fit to the data was subtracted and all the data were normalized at an energy 80 eV higher than the first inflection point. In order to calculate the pressure-induced charge transfer in $YBa_2Cu_3O_{7-\delta}$ we have used the intensity variations in the spectral feature at 1 eV corresponding to the monovalent Cu(1) atoms[27–30] in the Cu *K*-edge XANES of $YBa_2Cu_3O_{7-\delta}$. As the oxygen content in the compound is increased, the $Cu(1)^{1+}$ feature loses strength due a filling by electrons of the empty hybridized states associated with Cu(1). We identify this gain in electrons by Cu(1) with a hole transfer from Cu(1) to Cu(2) sites. Assuming a hole increase of 0.25 in the CuO_2 planes by increasing the oxygen content from 6.10 to 6.95,[48] the area difference of this spectral feature between the $\delta = 0.05$ and $\delta = 0.9$ compounds was used as a calibration in calculating the amount of the charge transfer induced by increasing the pressure from 1 bar to 65 kbar, for $YBa_2Cu_3O_{6.95}$. The area calculations, performed by applying a tenth order polynomial fit to the data around the $Cu(1)^{1+}$ feature, indicate a charge transfer of 0.0007 ± 0.0002 holes/kbar per CuO_2 plane for the $YBa_2Cu_3O_{6.95}$.

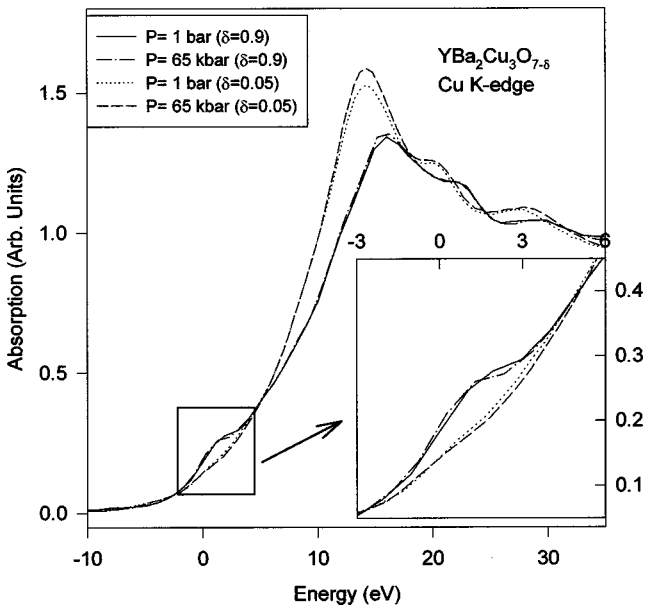

FIG. 8. Cu *K*-edge XANES of $YBa_2Cu_3O_{6.95}$ and $YBa_2Cu_3O_{6.10}$ at 1 bar and 65 kbar. The feature at 1 eV corresponds to $Cu(1)^{1+}$. The intensity variations of this feature between $YBa_2Cu_3O_{6.95}$ and $YBa_2Cu_3O_{6.10}$ are used as a calibration for the charge transfer from CuO chains to CuO_2 planes with pressure.

V. SUMMARY AND CONCLUSIONS

Our high pressure XAFS experimental results on $YBa_2Cu_3O_{6.95}$ indicate a buckling in the Cu(1)-O(4)-Cu(2) units through the O(4) atoms. Using multiple scattering analysis, it has been shown that the buckling angle (β) increases rapidly at low pressures then saturates at ~ 65 kbar. The magnitude of the saturation angle (β_{sat}) is dependent upon details of the EXAFS analysis. If the Cu(1)-O(4)-Cu(2) path is assumed to be linear at 1 bar, then β_{sat} is found to be 12°. If the presence of static or dynamical displacements of the O(4) atom from the *c* axis, as reported in ion channeling and neutron diffraction experiments at 1 bar, are included in the EXAFS analysis by assuming that the path is already buckled by 3° at atmospheric pressure then β still saturates close to 12°. But because of the limitations of the analysis method this may be an overestimate by as much as 3°. These results indicate a similarity between the structural distortions in $YBa_2Cu_3O_{7-\delta}$ and $La_{2-x}(Sr, Ba)_xCuO_4$ systems in which

a buckling structure was observed at ambient pressure[17,18] and high-pressure.[6]

The magnitude of the MS effect decreases as β increases. By 65 kbar it is no longer possible to separate the Cu(1)-O(4)-Cu(2) from the other contributions to the peak at 3.9 Å in the Fourier transform of the EXAFS interference function. Neutron diffraction may be able to follow the buckling into higher pressures.

The anisotropy of the pressure dependence of T_c has been reported from the discontinuities in the high resolution thermal expansion data. According to these studies the pressure derivative of T_c is large and opposite in sign along the *a* and *b* axes but small along the *c* axis leading to an overall low pressure dependence of T_c for $YBa_2Cu_3O_{7-\delta}$.[50] The buckling structure can have important aspects explaining these anisotropies. Burns,[51] proposing a coupling of superconductivity to the shear deformation along the [110], showed the dependence of T_c on shear stress (τ) increases up to a critical point at which $dT_c/d\tau=0$ and decreases with further increase in τ.

The buckling structure can also have a contribution to T_c according to the resonating valence bond of Anderson[52] in which the logarithmic volume derivative of T_c is related explicitly to carrier concentration and to the transfer integrals parallel ($t_\parallel$) and perpendicular ($t_\perp$) to the CuO_2 planes. With the distortion of the O(4) atoms $t_\perp$ is expected to decrease. However, the effect of this decrease on the pressure derivative of T_c is expected to be small since the dominant contribution to the change in T_c comes from the carrier concentration term according to this model.

XANES results suggesting a charge transfer of 0.0007 ± 0.0002 holes/kbar from chains to the planes agree with the neutron diffraction results,[5] but neutron diffraction does not observe buckling along the *c* axis. Other theories of the holes produced ignore the possibility of buckling, but their results bracket our XANES number.

ACKNOWLEDGMENTS

The authors wish to acknowledge W. N. Hardy for providing the $YBa_2Cu_3O_{7-\delta}$ samples and J. Franck for assistance with data acquisition. This work was supported by the Natural Sciences and Engineering Research Council of Canada and the U.S. Department of Energy Grant No. DE-FG06-84ER45613. Experiments were performed at Stanford Synchrotron Radiation Laboratory which is supported by the U.S. Department of Energy and the National Institute of Health.

[1] W. H. Fietz, M. R. Dietrich, and J. Ecke, Z. Phys. B **69**, 17 (1987).
[2] M. R. Dietrich, W. H. Fietz, J. Ecke, and C. Politis, Jpn. J. Appl. Phys., Suppl. **26**, 1113 (1987).
[3] H. Takayashi, C. Murayama, S. Yomo, N. Mori, W. Ustumi, and T. Yagi, Jpn. J. Appl. Phys., Suppl. **26**, 1109 (1987).
[4] N. V. Jaya, S. Natarajan, and G. V. S. Rao, Solid State Commun. **67**, 51 (1988).
[5] J. D. Jorgensen, S. Pei, P. Lightfoot, D. G. Hinks, B. W. Veal, B. Dabrowski, A. P. Paulikas, R. Kleb, and I. D. Brown, Physica C **171**, 93 (1990).
[6] N. Alberding, K. R. Bauchspieß, J. M. Tranquada, R. Ingalls, and E. D. Crozier, Physica B **158**, 463 (1989).
[7] M. J. Akhtar, Z. N. Akhtar, and C. R. A. Catlow, J. Phys.: Condens. Matter **2**, 3231 (1990).
[8] W. Shafer, E. Jansen, G. Will, J. Faber, and B. Veal, Mater. Res. Bull. **23**, 1439 (1988).
[9] M. Francois, A. Junod, K. Yvon, A. W. Hewat, J. J. Capponi, P. Strobel, M. Marezio, and P. Fischer, Solid State Commun. **66**, 1117 (1988).
[10] R. P. Sharma, F. J. Rotella, J. D. Jorgensen, and L. E. Rehn, Physica C **174**, 409 (1991).
[11] J. Mustre de Leon, S. D. Conradson, I. Batistic, and A. R. Bishop, Phys. Rev. Lett. **64**, 1675 (1990).
[12] J. Mustre de Leon, S. D. Conradson, I. Batistic, A. R. Bishop, I. D. Raistrick, M. C. Aronson, and F. H. Garzon, Phys. Rev. B **45**, 2447 (1992).
[13] E. A. Stern, M. Qian, Y. Yacoby, S. M. Heald, and H. Maeda, Physica C **209**, 331 (1993).
[14] C. H. Booth, F. Bridges, J. B. Boyce, T. Claeson, B. M. Lairson, R. Liang, and D. A. Bonn, Phys. Rev. B **54**, 9542 (1996).
[15] P. Schweiss, W. Reichart, M. Braden, G. Collin, G. Heger, H. Claus, and A. Erb, Phys. Rev. B **49**, 1387 (1994).
[16] M. Arai, K. Yamada, Y. Hidaka, S. Itoh, Z. A. Bowden, A. D. Taylor, and Y. Endoh, Phys. Rev. Lett. **69**, 359 (1992).
[17] R. J. Birgeneau and G. Shirane, in *Physical Properties of High-Temperature Superconductors I*, edited by D. M. Ginsberg (World Scientific, Singapore, 1989).
[18] J. D. Axe, A. H. Moudden, D. Hohlwein, D. E. Cox, K. M. Mohanty, A. R. Moodenbaugh, and Y. Xu, Phys. Rev. Lett. **62**, 2751 (1989).
[19] J.-E. Jørgensen, J. D. Jorgensen, B. Battlogg, J. P. Remeika, and J. D. Axe, Phys. Rev. B **33**, 4793 (1986).
[20] N. Alberding, E. D. Crozier, R. Ingalls, and B. Houser, J. Phys. (Paris), Colloq. **47**, C8-681 (1986).
[21] B. Houser, R. Ingalls, and J. J. Rehr, Physica B **208&209**, 323 (1995).
[22] F. S. Razavi, Z. Altounian, and W. R. Datars, Solid State Commun. **28**, 3762 (1978).
[23] B. Batlogg, R. G. Maines, M. Greenblatt, and S. Di Gregorio, Phys. Rev. B **29**, 3762 (1984).
[24] A. Di Cicco and M. Berretoni, Phys. Lett. A **176**, 375 (1993).
[25] J. J. Rehr, R. C. Albers, and S. I. Zabinsky, Phys. Rev. Lett. **69**, 3397 (1992).
[26] S. I. Zabinsky, A. Ankudinov, J. J. Rehr, and R. C. Albers, Phys. Rev. B **52**, 2995 (1995).
[27] S. Heald, J. M. Tranquada, A. R. Moodenbaugh, and Y. Xu, Phys. Rev. B **38**, 761 (1988).
[28] J. Röhler, A. Larisch, and R. Schäfer, Physica C **191**, 57 (1992).
[29] H. Tolentino, F. Baudelet, A. Fontaine, T. Gourieux, G. Krill, J. Y. Henry, and J. Rossat-Mignod, Physica C **192**, 115 (1992).
[30] L. B. Sorensen, J. O. Cross, M. Newville, B. Ravel, J. J. Rehr, H. Stragier, C. E. Bouldin, and J. C. Woicik, in *Resonant Anomalous X-ray Scattering-Theory and Applications*, edited by G. Materlik, C. J. Sparks, and K. Fischer (Elsevier Science, British Vancouver, 1994).

[31] P. Schleger, W. N. Hardy, and B. X. Yang, Physica C **176**, 261 (1991).
[32] K. R. Bauchspieß, Ph.D. thesis, Simon Fraser University, 1990.
[33] K. R. Bauchspieß, E. D. Crozier, and R. Ingalls, J. Phys. (Paris), Colloq. **47**, C8-975 (1986).
[34] E. D. Crozier and A. J. Seary, Can. J. Phys. **59**, 876 (1981).
[35] D. E. Sayers and B. A. Bunker, in *X-ray Absorption: Principles, Applications, Techniques of EXAFS, SEXAFS, and XANES*, edited by D. C. Koningsberger and R. Prins (Wiley, New York, 1988).
[36] M. Newville, P. Lìvinš, Y. Jacoby, J. J. Rehr, and E. A. Stern, Phys. Rev. B **47**, 14 126 (1993).
[37] K. R. Bauchspieß, Jpn. J. Appl. Phys. **32**, 131 (1993).
[38] H. Olijnyk, S. K. Sikka, and W. B. Holzapfel, Phys. Lett. A **103**, 137 (1984).
[39] N. Alberding and E. D. Crozier, Phys. Rev. B **27**, 3374 (1983).
[40] E. D. Crozier, Nucl. Instrum. Methods Phys. Res. B **133**, 134 (1997).
[41] M. Benfatto, C. R. Natoli, and A. Filipponi, Phys. Rev. B **40**, 9626 (1989).
[42] G. G. Li, F. Bridges, and C. H. Booth, Phys. Rev. B **52**, 6332 (1995).
[43] T. Ressler, M. Hagelstein, U. Hatje, and W. Metz, J. Phys. IV **C2**, 731 (1997).
[44] J. B. Boyce, F. Bridges, T. Claeson, and M. Nygren, Phys. Rev. B **39**, 6555 (1989).
[45] E. D. Crozier, N. Alberding, K. R. Bauchspieß, A. J. Seary, and S. Gygax, Phys. Rev. B **36**, 8288 (1987).
[46] R. P. Sharma, L. E. Rehn, P. M. Baldo, and J. Z. Liu, Phys. Rev. B **40**, 11 396 (1989).
[47] C. C. Almasan, S. H. Han, B. W. Lee, L. M. Paulius, M. B. Maple, B. W. Veal, J. W. Downey, A. P. Paulikas, Z. Fisk, and J. E. Schirber, Phys. Rev. Lett. **69**, 680 (1992).
[48] R. P. Gupta and M. Gupta, Phys. Rev. B **51**, 11 760 (1995).
[49] A. P. Reyes, E. T. Ahrens, P. C. Hammel, R. H. Heffner, and M. Takigawa, in *Proceedings of the Conference on Lattice Effects on High-T_c Superconductors*, edited by Y. Bar-Yam, T. Egami, J. Mustre de Leon, and A. R. Bishop (World Scientific, Singapore 1992).
[50] C. Meingast, O. Kraut, T. Wolf, H. Wühl, A. Erb, and G. Müller-Vogt, Phys. Rev. Lett. **67**, 1634 (1991).
[51] S. J. Burns, Physica C **206**, 97 (1993).
[52] P. W. Anderson, Science **235**, 1196 (1987).